4. Evolution of a fault-surface from 3D attribute analysis and displacement measurements

Abstract

A large fault-surface evolves by the growth and coalescence of numerous segments through time, which results in a strong undulation of the principal fault-surface on different scales. We interpreted a strongly segmented, approx. 13 km long fault in detail using 3D seismic data, and studied the fault-morphology in terms of fault-linkage, using attributes such as curvature, azimuth, and dip. Displacement profiles of two horizons have been measured in order to analyse the slip-throw-heave relation, and to quantify their variation and their dependence on the fault-morphology. The displacement profiles are triangular to half-elliptical in shape, rather than elliptical. This is clearly visible in slip but less in heave or throw. Our results illustrate that throw or heave may not be representative for displacement measurements along a fault, because segmented and strongly undulated faults show a strong variation in slip, throw, and heave. Additionally, the often-used heave or throw values lead to a smoothing of the displacement curves, and cannot show triangular-shaped curves due to the under-representation of slip. Morphological analyses and slip distribution of large-scale faults is important for a better understanding of the heterogeneous distribution of earthquake data, and to improve seismic hazard assessments.

4.1. Introduction

Faults grow most effectively by the coalescence of several smaller faults, whereas tip propagation is of only minor importance (e.g. Peacock and Sanderson, 1991; Willemse, 1997; Cartwright at al., 1995). Due to this coalescence of numerous segments through time, a fault's shape can strongly undulate, and the stress perturbations during fault interaction and increasing displacement result in a heterogeneous distribution of fractures at a smaller scale. Large-scale active faults are zones of potential seismicity; and together with their small-scale fracture network they can act as fluid conduits or barriers. The 3D fault-shape, the linkage of a fault with other faults, and the distribution of slip on its surface are important for defining the positions of juxtaposed beds that control, for example, connectivity and permeability across faults. Consequently, for the characterisation of reservoirs, the analysis of fluid transport, the precise placement of wells, as well as for estimating the potential of earthquake generation, it is very important to have detailed information about the 3D shape of large-scale faults in the subsurface.

Undulation of a fault surface results in differences between the vertical component (throw), and the horizontal component (heave) of the displacement, with respect to slip, the real displacement on the fault. Data used for investigation of fault geometry and fault statistics are often 2D (field data, remote sensing, seismic lines). Even when 3D data are available, faults are often studied in 2D only (horizon interpretation or cross-sections of 3D seismic data). However, the shape of an isolated normal fault is more complex as shown in previous papers (e.g. Walsh and Watterson, 1989; Nicol et al., 1996; Needham et al., 1996; Walsh et al., 1999).

In carrying out fault analysis, fault growth evolution is generally inferred from the geometrical characteristics of differently sized faults in the same population, rather than from kinematic analyses of individual faults. Many authors use throw or heave as approximation for slip, to

analyse fault-populations in terms of fault-propagation through time, length vs. displacement relationship, or displacement vs. cumulative frequency (e.g. McLeod et al., 2000; Meyer et al., 2002; Walsh et al., 2002; Nicol et al., 2005). Using throw or heave can be an approximation to slip in case of homogeneous lithology, low fault-segmentation, and smooth fault-surfaces. Calculation of throw and heave is also less time-consuming with respect to slip, especially for investigation of large faults, or fault-populations. However, as individual fault surfaces can undulate strongly, such simplified analyses might not always represent exact fault characteristics, which become more important for economic applications.

The high complexity of fault-growth in time and space requires a detailed analysis in 3D. On the basis of 3D seismic data we studied a c. 13 km long synsedimentary fault in detail, and analysed the fault-morphology and displacement distribution along the fault. We illustrate that the displacement pattern is very heterogeneous, which results in different shaped displacement curves (triangular, half-elliptical, or elliptical), depending on slip, throw, or heave. Additionally, throw or heave values may not be representative for the real kinematic displacement (slip) along the fault because of their strong variation due to fault segmentation.

4.2. Data Base and Methods

The study area is located in the NW German Basin, as part of the intracontinental Southern Permian Basin. In Central Europe, rifting and associated volcanism in the Permian occurred in a dextral transtensional stress regime (e.g. Ziegler, 1990) and produced mainly N-S striking normal faults, but also NW-trending dextral strike-slip faults (e.g. Betz et al., 1987; Ziegler, 1990; Kockel, 2002). This deformation event is well documented in our working area, expressed by grabens and halfgrabens containing Permian growth-strata (Lohr et al., 2007). Sandstone, fanglomerates, and volcanic rocks have been identified by well data.

We analysed a pre-stack depth-migrated 3D reflection seismic data set, provided by RWE Dea AG, Hamburg. The line spacing of the seismic volume is 25 m, with c. 30 m vertical resolution for the depth of the analysed fault. We concentrated our analysis on the detailed interpretation of one synsedimentary normal fault (c. 13 km length) and two horizons (h2 - Top Rotliegend, h1 - Base Rotliegend) (Fig. 4.1). The fault interpretation is based on detailed picking of every third seismic line (75 m interval) perpendicular to fault-strike, numerous lines oblique to fault-strike, and horizontal correlations on depth slices.

We interpreted the seismic data with the Schlumberger software GeoFrame. Triangulation of surfaces and fault attribute analyses were carried out with the software package GoCad (GOCAD Consortium). The Midland Valley software 3Dmove was used for displacement measurements.

After interpretation of the seismic data in terms of horizons and faults, we created a 3D fault-surface by using the GoCad triangulation method (homogeneous triangles, Fig. 4.2). Subsequently, we analysed the fault-topography by using the attributes dip, azimuth, and curvature. The real dip and azimuth are calculated from each triangle of the fault-surface. The Gaussian curvature at a given point is the product of the two principal maximum and minimum curvatures. By flattening the 3D triangular grid, positive curvature is defined by a gap forming between flattened triangles of a dome, whereas negative curvature is defined by an overlap forming between flattened triangles of a saddle or basin. Surfaces with a high Gaussian curvature like domes or saddles are non cylindrical, whereas cylindrical surfaces like elongated folds have a Gaussian curvature of zero (Lisle, 1994).

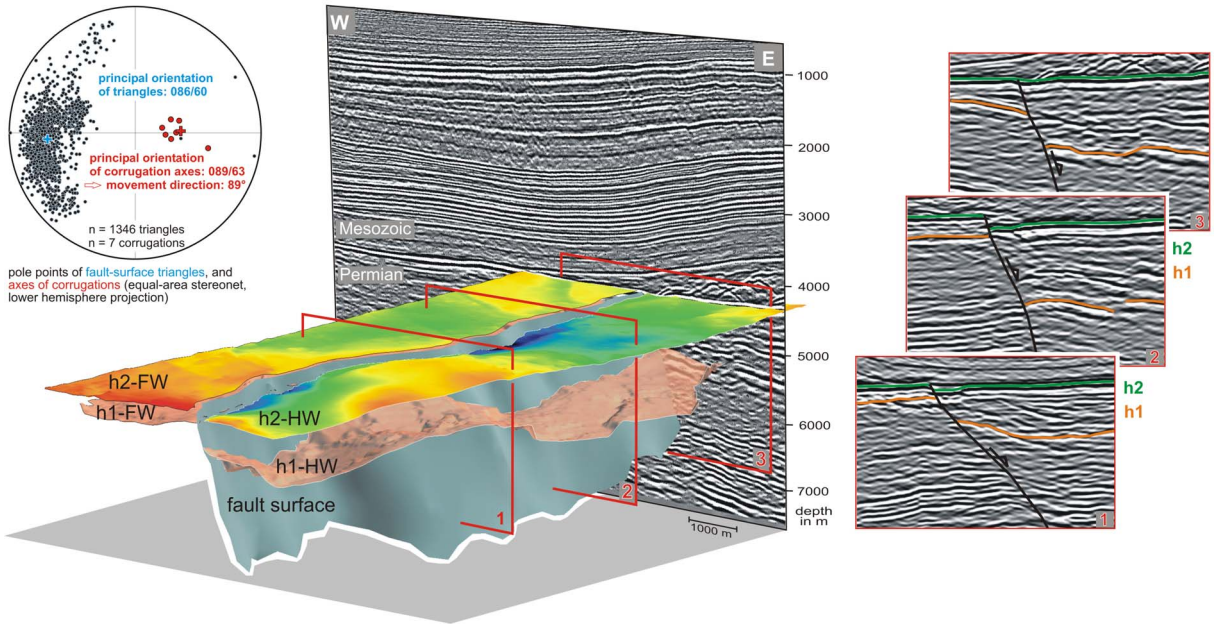

Figure 4.1: 3D view showing the structural model with the analysed fault, two horizons (h2 is Top Rotliegend, h1 is Base Rotliegend), and several seismic sections. FW = footwall, HW = hanging wall. H2 horizon is colour-coded with depth, from red to blue. View towards the NW. No vertical exaggeration. Left: Equal-area stereonet plot of poles, demonstrating the variation in dip and azimuth of each fault-triangle, and showing the axes of corrugations.

The attributes dip, azimuth, and curvature can highlight corrugations on the fault-surface. These attributes vary independently from the sections on which the fault has been interpreted, and are therefore a real feature rather than an artefact of the interpretation. These fault-corrugations are assumed to result from segment linkage (e.g. Walsh et al, 1999; McLeod et al., 2000; Mansfield and Cartwright, 2001; Marchal et al., 2003); they also indicate the movement direction as parallel to the axis of the corrugations, because this movement should require least energy and therefore smallest strain (Needham et al., 1996). Such corrugations have been observed also in the field (e.g. Wright and Turner, 2006; Sagy et al., 2007), and can be interpreted as fault-segments and fault-segment linkage zones. Striation measurements on these corrugations evidenced that corrugations are parallel to fault slip (Hancock and Barka, 1987). These corrugations observed in the field might be comparable to those observed in seismic data.

Thus, we used the here observed corrugations to define the movement direction on the fault. For the subsequent displacement measurements we calculated the amount of slip, heave and throw between the fault-surface and two Permian horizons: We mapped in detail the positions of the hanging wall and footwall cut-offs on the fault-surface (by directly "snapping" in the seismic interpretation software), defined the movement direction on the fault from the fault-corrugations (average movement direction is 89°, Fig. 4.1), and subsequently measured the displacements using the 3Dmove module "Allen Mapper". For this purpose, a vertical plane trending parallel to the movement direction was shifted step by step along the fault, rasterising the fault in numerous cross-sections (180 at h1, 250 at h2) and measuring the three displacement components.

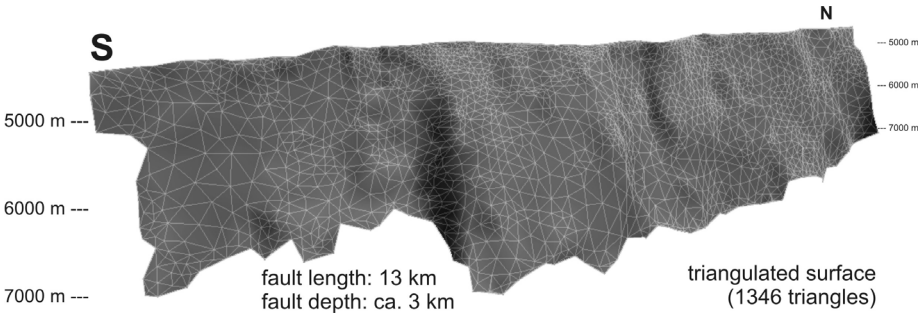

Figure 4.2: 3D view of the analysed fault-surface. View toward the NW. No vertical exaggeration.

4.3. Fault analysis

The studied fault strikes N-S and dips toward the east (Fig. 4.1). The fault is accessible almost in its complete extent in the seismic data set. The northern bound is limited by the margins of the seismic volume, whereas the southern bound is limited in interpretation by an overlaying Zechstein salt diapir. The fault is picked in a depth from 4200 m down to 7500 m (Fig. 4.2); the minimum value is defined by the blind upper fault tip because of the end of deformation, and the maximum value is given by the depth limit of the seismic volume (Fig. 4.1). The southernmost part of the investigated fault has been affected by later faulting. These areas were not involved in our analysis.

We studied the fault-morphology (Fig. 4.2) in two different ways: fault attribute analyses (dip, azimuth, curvature) highlight fault-corrugations in 3D at a larger scale of several kilometres. In contrast, displacement measurements can emphasise fault-corrugations only in 2D, but on a smaller scale of a few 100 metres to several kilometres. The results of both methods are appropriate to analyse the fault-morphology over a larger scale spectrum.

4.3.1. Large-scale fault analysis

Analysing the fault-morphology in 3D, we observed an undulation of the whole fault (Fig. 4.1, 4.2), expressed already by differences in orientation of the numerous fault-surface triangles.

The *dip* and *azimuth* maps and their histograms illustrate these differences (Fig. 4.3). The fault-dip varies between 35° and 80°. The average dip is 60°, but there are two main clusters with an average dip of 42° and 65° respectively. The average azimuth is 86°, but it varies between 40° and 165°. Comparing the dip and azimuth histograms (Fig. 4.3) with the dip-azimuth pole plot (Fig. 4.4) it is possible to assign fault regions to clusters of the pole plot. Density contour lines highlight several clusters (1 to 4), which correspond to several dip or azimuth clusters in the histogram, and to several regions in the fault attribute maps: cluster 1 corresponds to the majority of high-dip areas in the north and the south, cluster 2 is the low-dip area in the middle of the fault (overlap zone), cluster 3 represents the southernmost parts of both second-order faults (explained in chapter 4.3.2.), and cluster 4 is related to a possible transfer zone (explained in chapter 4.4.1.)

The Gaussian *curvature* was calculated for the whole fault surface. The undulation of the fault surface is not homogenous in both directions, but it is elongated sub-parallel to fault-dip, and the fault can therefore be described as a cylindrical surface. For that reason we used the minimum Gaussian curvature since it highlights well the corrugations on this surface (Fig. 4.3). Areas of positive curvature are convex to the hanging-wall, and represent areas where fault-linkage

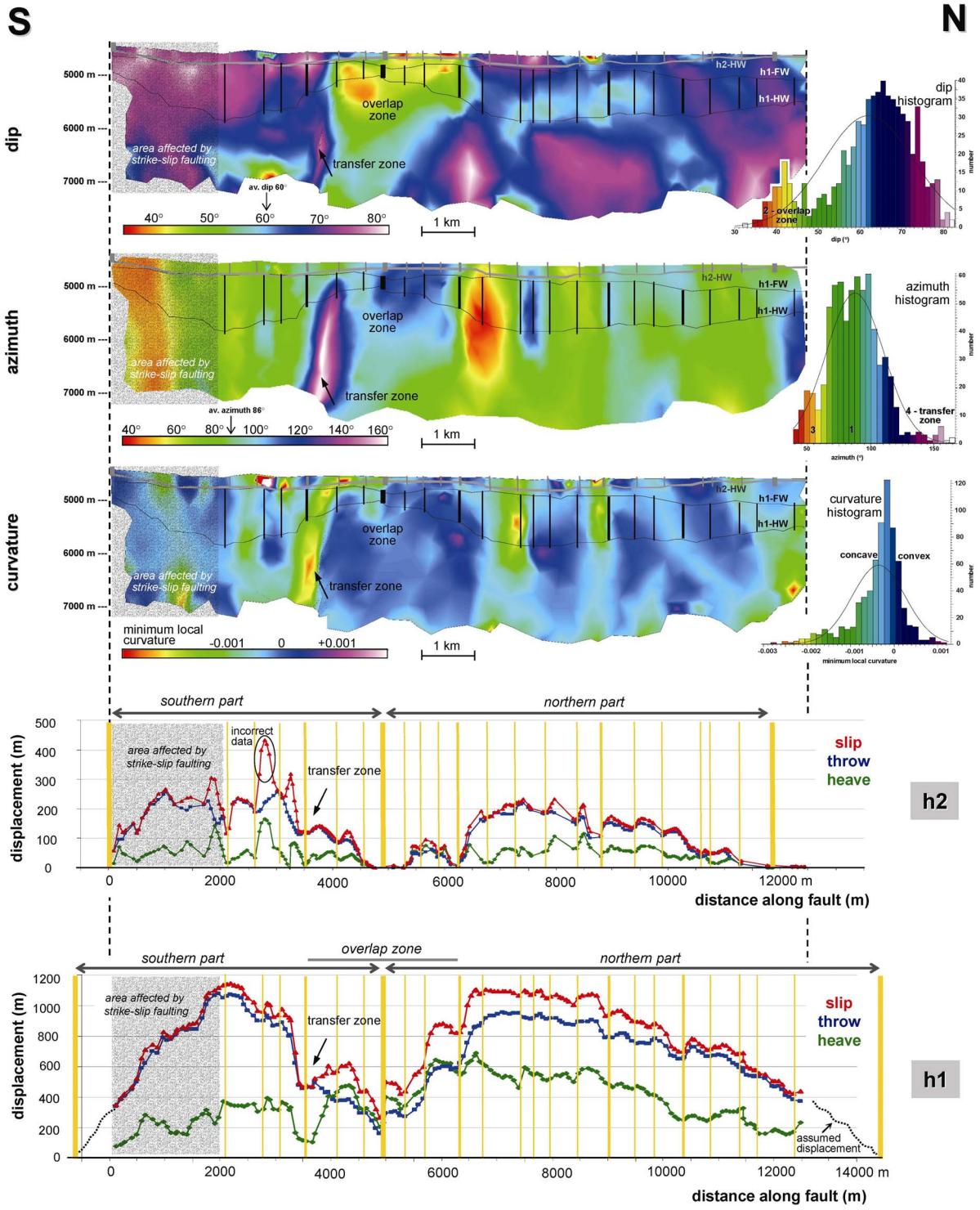

Figure 4.3: Top: Fault surface as colour-coded attribute maps showing dip, azimuth, and curvature, with corresponding histograms. View towards the fault-surface. Horizontal undulated lines are hanging wall and footwall cut-off of h1 (black lines, h1-HW and h1-FW), and hanging wall cut-off of h2 (grey line, h2-HW). Straight vertical lines between the cut-offs represent segment boundaries interpreted from the diagrams below. Numbers in histograms are related to the several clusters in Figure 4.4.
Below: Displacement-distance diagrams of the two Permian horizons (h1 - Base Rotliegend, h2 - Top Rotliegend) showing their separation along fault. Coloured lines indicate slip, throw, and heave. Variations of these lines reflect different fault-segments, which have been linked during fault-propagation, and finally produced one large fault-surface. Vertical yellow lines in the diagrams are fault-segment boundaries. Segments between thinner lines are smaller and older, whereas segments between thicker lines are larger and younger segments, which developed from linkage of the smaller ones. According to this subdivision four generations of fault-growth are identified.

occurred. Areas of negative curvature are concave to the hanging-wall, and represent the fault-segments itself (Fig. 4.3). In the histogram the average minimum local curvature is shifted to more negative values, which means that concave areas, and thus fault-segments, are overrepresented with respect to the convex ones (fault-linkage areas). That is reasonable as fault-segments are usually larger than zones of fault-linkage. The high curvature areas are not continuously visible along fault-depth. Comparing both, dip and curvature map, indicates that areas of high negative curvature are represented by higher dip, with respect to their surroundings, and that corrugations become narrower or die out towards the depth; some of them even at the same depth level of about 6000 m (Fig. 4.3).

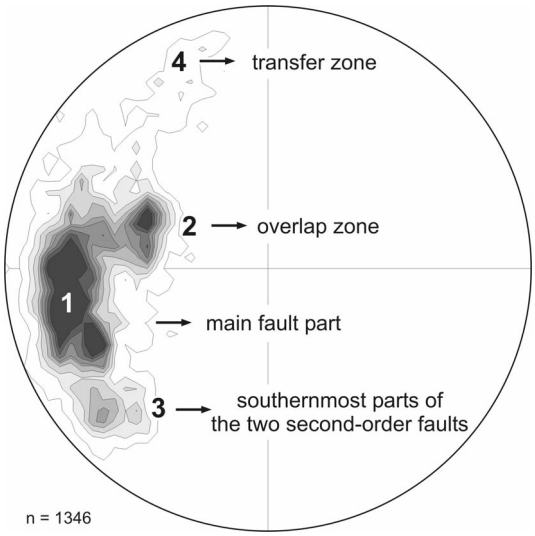

Figure 4.4: Equal-area stereonet plot with contour lines shows the distribution in orientation of fault-surface triangles derived from pole point plot in Figure 4.1. The four identified clusters have been correlated with areas on the fault-surface (compare with Figure 4.3).

Subordinate to these vertical corrugations we also note horizontal corrugations (Fig. 4.3, e.g. at ca. 5000 m depth level between 7000 and 10000 m distance along the fault). The hanging wall and footwall cut-off lines often match with areas of strong changes in dip or curvature, e.g.: the large horizontal corrugation visible as a low-dip area within the northern part of the fault is located between the hanging wall and footwall cut-offs of horizon h1; the hanging wall cut-off of this horizon often limits areas of high negative curvature at depth (Fig. 4.3, e.g. at 3600, 7400, 8900 m distance along the fault). The uppermost part of the fault surface (the area between hanging wall and footwall of horizon h2) is characterised by several small areas of changes in dip and curvature. This implies higher fault roughness in this upper part compared to deeper areas.

4.3.2. Small-scale fault analysis

For a more detailed investigation of fault-corrugations we measured the displacement of two horizons (h1 - Base Rotliegend, h2 - Top Rotliegend) along the fault. We analysed the amount of throw (vertical component of displacement), heave (horizontal component of displacement), as well as slip (real displacement) along the fault. The results are shown in the displacement-distance diagrams (Fig. 4.3) that illustrate the displacement-variation parallel to fault-strike. Profiles of both horizons are asymmetric, triangular to elliptical, convex-shaped curves. The displacement varies between 0 and 1200 m in h1, and between 0 and 300 m in h2. The curves show several sub-units with local minima and maxima, which point to different segments, that merged during fault growth. Maxima represent the core of the fault-segments because maximum displacement occurred close to the centre of the segments, whereas minima represent areas where fault-segments are linked because displacement is tapering off at the edges. Minima are also characterised by abrupt changes in displacement. Their positions are similar in the throw, heave,

and slip curves, but the amounts of displacement are different between these curves, which results in a different slip-throw-heave relationship of each segment. Based on the distribution of minima and maxima, we identified four generations or orders of segments on both horizons (Fig. 4.3). These are younger with increasing fault-length, because of progressive fault-growth by segment linkage.

Fourth-order:	more than 23 small-scale segments (200 - 700 m length)
Third-order:	at least 6 medium-scale segments (1.5 - 3 km length)
Second-order:	2 large-scale segments (5 - 9 km length)
First-order:	1 large-scale final fault (c. 13 km length)

Vertical yellow lines in the diagrams separate these segments. Segments between thinner lines are smaller and older, whereas segments between thicker lines are larger and younger segments. The first-order fault has a length of approx. 15 km at horizon h1, and 12 km at horizon h2. The two second-order faults are well visible on the present-day morphology of the h2 hanging wall (Fig. 4.1). Here, the depth map shows two areas of increased depths (blue coloured), which indicate maximum subsidence and displacement along horizon h2 (fault-controlled depocentres). The area between both second-order faults appears as overlap zone, bounded by a transfer zone to the south (Figs. 4.2, 4.3). Third-order faults are in the scale of a few kilometres, and the numerous fourth-order faults with several hundred metres length are the smallest segments that could be identified by this method.

Areas of segment linkage identified from the displacement-distance diagrams match with areas of strong differences in dip, azimuth, or curvature, identified from fault-morphology analysis (Fig. 4.3). In the dip map the vertical lines often separate horizontal neighbours of varying dip. The colour bar of the azimuth map highlights especially areas which strike oblique to the major fault, so that green coloured areas represent mainly fault-segments. In the curvature map, most of the fault-segments are directly visually enhanced by the negative curvature values presented in red, yellow and green colours. Nearly all segment boundaries from the diagrams have been identified also on one or more fault attribute maps. However, a few fourth-order segments could not be correlated with fault attribute maps. This might be because the displacement-distance diagrams can identify fault-segments on a much smaller scale. In general, the fault-surface roughness seems to change with depth. The upper part of the fault-surface between the hanging wall and footwall of h2 is characterised by a higher amount of small fault segments with respect to the area of h1. In h1 small segments can only be identified in the displacement-distance diagram in such detail, but rarely on the attribute maps.

The fault-morphology, especially the changes in dip, controls the slip-to-throw ratio. We calculated this ratio for the oldest horizon h1 (Fig. 4.5). Here, the slip-to-throw ratio varies along fault-strike between 1 and 1.8. The curve is strongly undulated and describes mainly concave shapes, which are separated by local maxima. These local maxima can be correlated in most cases with zones of segment linkage derived from the displacement-distance diagram (Fig. 4.3). The highest slip-to-throw ratio occurs within the large overlap zone, in which the second-order fault segments are linked. The reason for this correlation is that fault-segment boundaries have typically lower fault-dip and smaller displacement with respect to the segment centre, which results in a higher slip-to-throw ratio.

Figure 4.6 shows the amount of throw and heave with respect to slip of all data pairs along both horizons. Comparing the three curves indicates that they are not sub-parallel as it would be the case on a planar fault-surface. Instead, throw and heave strongly undulate in comparison to slip. In some cases, heave is even higher than throw. This occurs when the fault-dip is locally below

45°, as it is the case in the area of the overlap zone (see dip map in Fig. 4.3). The higher the differences between throw and heave, the steeper the fault is. The heterogeneity in the displacement curves are mainly caused by fault-segmentation and the related undulation of the fault-surface. Additionally, the slip curve in this diagram (Fig. 4.6) is not a continuous line, but it is marked by steps of some tens of metres. These steps divide the curve into groups of similar slip, but the relation between throw and heave often varies.

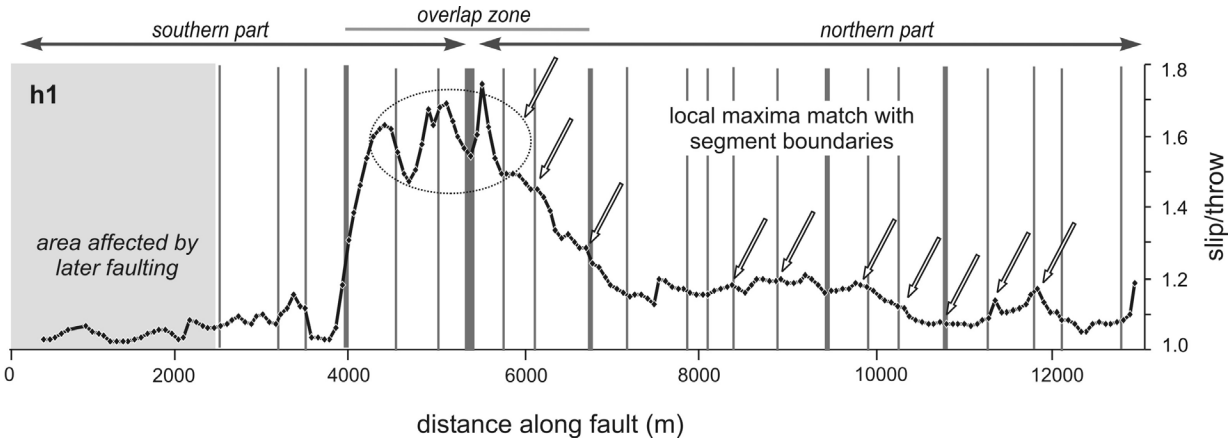

Figure 4.5: Slip/throw ratio of horizon h1. Vertical lines are segment boundaries derived from the displacement-distance diagram in Figure 4.3. In general, high ratios point to segments boundaries, whereas low ratios indicate fault segments. Here, arrows mark such maxima that correlate with segment boundaries.

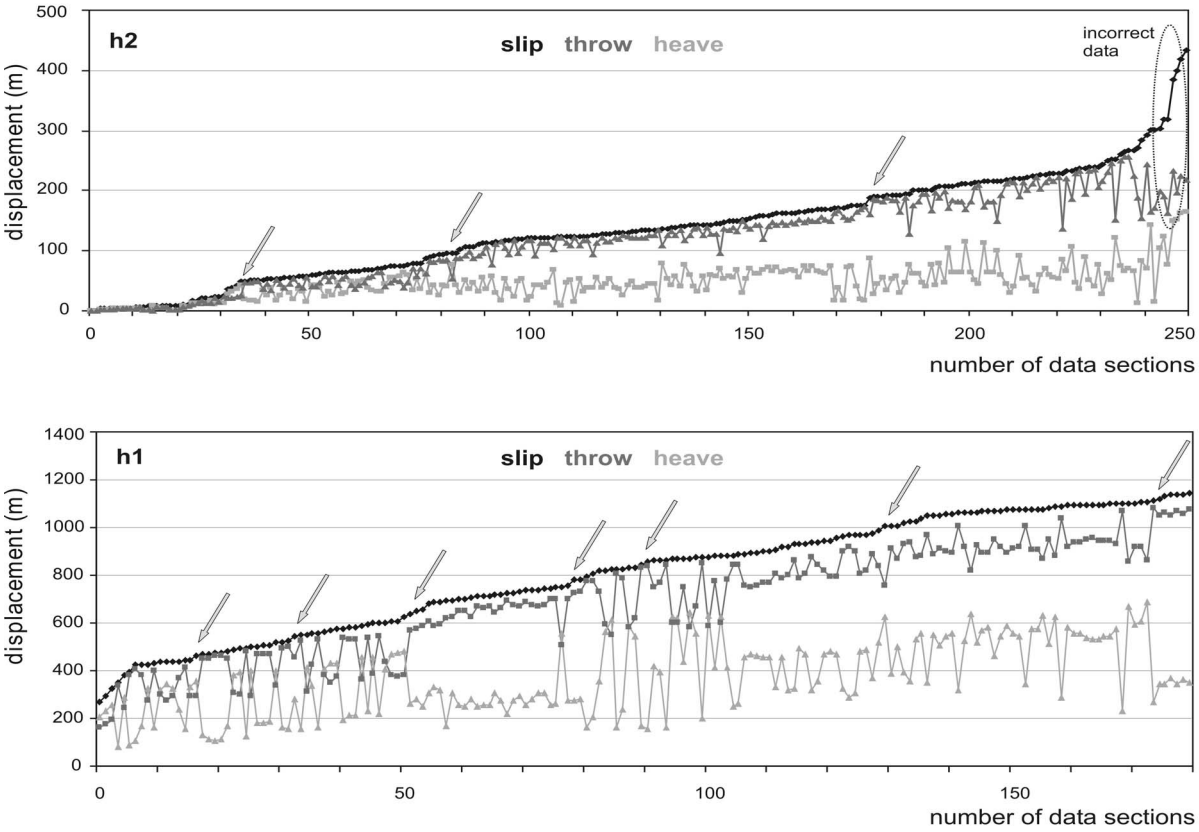

Figure 4.6: Variation of throw and heave with respect to slip. Data pairs of both horizons are ordered by slip. Steps in curve represent groups of segments with similar displacement pattern.

4.4. Discussion

4.4.1. Fault corrugations and displacement calculations

With the here used methods of 3D fault interpretation and subsequent attribute analysis and displacement measurements, we identified corrugations as former segments on a present-day large fault-surface, over a scale range from a few hundred metres to several kilometres. The consistency in interpretation results over that range of scales and demonstrates the validity of the two methods. We assume that the here analysed fault formed from smaller faults, which coalesced during fault-propagation in the Permian.

On a km-scale attribute analysis of the fault-surface highlights undulations or corrugations, which we interpret to represent former fault-segments and fault-linkage. Areas of negative curvature, which are concave to the hanging-wall, are interpreted as fault-segments. Areas of positive curvature, which are convex to the hanging-wall, are interpreted as breached relay zones where fault-linkage occurred. One example of negative curvature even highlights a possible transfer zone, which might indicate a breached relay ramp (Fig. 4.3). The fault-corrugations identified by attribute analyses are sub-parallel to fault dip, and are assumed to be aligned parallel to slip direction (also Needham et al., 1996).

By displacement analysis on a scale of a few hundred metres to several kilometres we identified four orders of segments illustrating different fault generations, getting younger with increasing fault-length. Each segment has its own slip-throw-heave relationship, which is mainly caused by differences in fault-strike and -dip, along both fault-strike and fault-depth (compare displacement-distance diagrams with fault attribute maps in Fig. 4.3). Differences along strike are caused by lateral coalescence of several segments (see also Needham et al., 1996; Marchal et al., 2003), whereas differences towards depth might be caused by vertical coalescence of several segments (Mansfield and Cartwright, 2001; Marchal et al., 2003), or by lithological inhomogeneities (Crider and Peacock, 2004), or a combination of both.

Our analyses show that the fault-surface topography evolves with increasing slip. Since we observed a variable fault-roughness associated with the horizon cut-offs rather than with depth, we assume that this roughness is related to displacement, rather than lithological inhomogeneities, or even interpretation uncertainties due to lower resolution at depth. In the here analysed scale the fault smoothes with increasing displacement. Therefore, we assume that coalescence of several segments leads first to an increase in fault-roughness, whereas during maturation the fault-surface becomes smoother. From outcrop data Sagy et al. (2007) also implied that mature fault-surfaces are smoother at small scales, and that slip correlates with fault-roughness.

The curves of the second-order, and partly the third-order segments are characterised by an asymmetric shape. The overlapping fault-tips have steeper displacement gradients than the corresponding distal tips (Fig. 4.3). This asymmetric fault-growth is caused by different fault-length propagation at both sides of the fault. During length propagation, the overlapping tips are hampered, but the free ends of the faults do propagate normally, as well as the growth in displacement is the same. This distortion of the displacement profile is typically observed in fault interactions (e.g. Peacock and Sanderson, 1991; Scholz, 2002).

The asymmetry in displacement-distribution of the smaller segments is caused by a higher displacement in the centre of the superimposed fault. The positions of displacement maxima are similar in both horizons, and the positions of third- and fourth-order segment boundaries are

mainly coincident. However, the first-order fault boundaries do not match, because the fault-length is smaller at the younger horizon h2 (12 km), than at the older horizon h1 (15 km) (Fig. 4.3). That indicates that in this observable deformation stage, the fault propagated only in displacement, but no tip propagation at the free ends of the fault has occurred.

4.4.2. Implications for fracture prediction, scaling, and seismic hazard assessment

The variable displacement along fault-strike caused by segment linkage, and the variable slip/throw/heave relations caused by differences in segment orientation, can result in heterogeneous deflections of horizons close to the fault, and should therefore have an influence on different fault drag geometries along the fault (reverse or normal drag). Barnett et al. (1987) suggested that different drags result from a local decrease or increase in displacement in fault-dip direction, and also Grasemann et al. (2005) argued that the sense of fault drag is mainly a function of the angle between the horizon and the fault plane, and therefore of the variation in fault-dip.

Care should be taken when calculating the length vs. displacement relationships, displacement vs. cumulative frequency relationships, or displacement through time, especially for a predictive purpose. An ideal self-similar growth is rarely observed; there is a lot of scatter in displacement-length correlation plots, which is caused by the process of segment linkage (Cartwright et al., 1996; Mansfield and Cartwright, 2001), and maybe also due to the use of throw and heave values rather that slip. Because of strong differences in slip, throw, and heave of mature, high-undulating faults, it is necessary to use slip values as they represent the real displacement. Otherwise, the use of heave and throw values lead to underestimation of the real fault-displacement. To work out the precise effects, it would be necessary to calculate the length vs. displacement relationship over time for all segments of one fault. However, in a segmented fault, the original lengths and displacements of the several segments are difficult to reconstruct, because they are underrepresented due to linkage. The present-day observable fault-lengths and fault-displacements in the displacement-distance diagram are slightly smaller than in reality, because they are related to a certain horizon that may not indicate the beginning of deformation. The solution would be to interpret for each segment that horizon which documents the beginning of faulting. However, in our example there is a lack of continuous and datable horizons for doing such detailed interpretations. Furthermore, the here analysed fault is not large enough for documenting a statistically relevant number of fault-segments. For these reasons, it was not possible to demonstrate specific implications on e.g. displacement-length scaling law between length vs. slip, length vs. throw, and length vs. heave in the here introduced example.

According to the inhomogeneous fault-roughness, the rocks around the fault should show an inhomogeneous strain field with high fracture concentration in areas of strong fault undulations (high curvature) (Lisle, 1994). Fault zones of high curvature are affected by higher deformation, and are therefore characterised by a higher fracture density. Hence, a large segmented fault shows a variable fracture density along both fault-strike and fault-depth. From fault analysis on the here studied scale, it might be possible to make qualitative predictions about fracture density around the major fault also on a much smaller scale, e.g. below the seismic resolution down to a few metres or even well data scale. This finally helps to localise strongly fractured zones, which is important for analyses of fluid migration and for reservoir characterisation.

Our analyses show triangular- to half-elliptical-shaped displacement profiles, clearly visible in slip, but rather in heave or throw. A triangular shape of displacement profiles is considered typical for long-term slip profiles derived from multiple rupture-surfaces from earthquake processes (e.g. Nicol et al., 1996; Manighetti et al., 2001, Manzocchi et al., 2006). However, this triangular shape

from seismological analyses has not been shown by analyses from seismic data; instead, in these studies fault-growth is typically characterised by an elliptical to half-elliptical displacement curve (e.g. Meyer et al., 2002; Nicol et al., 2005; Bull et al., 2006). A reason for this discrepancy could be that fault-growth evolution has generally been inferred from the geometrical characteristics of faults of different size in the same population, rather than from kinematic analysis of an individual fault. Displacement profiles of one single mature fault change continuously through time due to segment linkage. Neighbouring faults act as barriers and hamper tip propagation, which results in a higher displacement gradient and necessarily a more triangular curve. However, the often used heave or throw values generate only an elliptical to half-elliptical shape due to under-representation of slip by constant fault-length, as it is illustrated in our displacement profiles (Fig. 4.3). Additionally, the use of only 2D seismic profiles, instead of a complete 3D interpretation, lowers the sampling rate significantly, which results in (1) a smoothing of the displacement curves, (2) an incomplete identification of fault segments, and (3) a nearly impossible recognition of a potential triangular-shaped curve. In the latter case, a triangular curve can only be identified in 2D interpretations by chosen the exact position of maximum displacement, and in addition numerous profiles around to prove the displacement gradient towards the fault tip. With this method, a triangular curve can only be identified by chance.

Analyses of the morphology of large faults are important for improvement of seismic hazard assessments. From seismological data, inhomogeneities on large-scale fault-surfaces are known as asperities. These asperities are described as areas of higher resistance against the general motion, caused by structural heterogeneities or varying material properties (Sobiesiak, 2005). During rupturing of asperities, these areas are characterised by an increased seismicity and higher slip values. Fault-morphology analyses could help to identify areas with high earthquake potential of seismic active faults, and to elucidate better the rupture process along the surface. However, for testing the comparability of the fault-surface roughness with the seismological potential, it is necessary to apply both analyses, 3D seismic and seismological data, on one single large-scale fault in very detail. If areas of increased slip correlate in both methods, and areas of segment linkage correlate with asperities, than the here introduced fault-morphology and displacement analysis from 3D seismic data will be an important contribution for the improvement of seismic hazard assessment.

4.5. Conclusions

(1) In this study we demonstrate fault-analysis of a c. 13 km long segmented fault, derived from detailed interpretation of a high-resolution 3D seismic data set. Here, we present for the first time the evolution of fault-segmentation on a single normal fault, with the combined methods of morphology analysis (dip, azimuth, and curvature attributes) and displacement measurements. We identified four orders of segments on two horizons getting younger with increasing fault-length, over several scales from 200 m to 15000 m fault length.

(2) Fault attribute maps (dip, azimuth, curvature) and displacement diagrams emphasise changes in fault-strike and fault-dip of the fault-surface. Our analysis shows a strong variation in slip, throw, and heave, especially in areas where fault-segments are linked. The difference in the amount of displacement increases with undulation along fault-strike and fault-dip. Consequently, throw and heave should not be used as approximation of slip, and are not representative for fault-analysis (e.g. fault-propagation through time, length vs. displacement relationship, displacement vs. cumulative frequency) of large segmented faults. Otherwise, high amounts of slip will be under-represented.

(3) Fault-morphology analyses of large-scale faults can be important for improvement of seismic hazard assessments, as the fault-roughness is possibly associated with the heterogeneous distribution of earthquake data.

(4) The here presented slip profiles are characterised by a triangular to half-elliptical shape, rather than being elliptical. We assume that the use of 2D profiles instead of 3D data, and the use of heave and throw instead of slip, leads to an incomplete identification of fault-segments, and therefore results not only in a smoothing of the curves, but also in a change from triangular to (half-) elliptical displacement curves. Hence, the high complexity of fault-growth in time and space requires a detailed analysis in 3D.